UC Riverside
UC Riverside Previously Published Works

Title

Dual feedback inhibition of ATP-dependent caffeate activation economizes ATP in caffeate-dependent electron bifurcation.

Permalink

https://escholarship.org/uc/item/8v66w2gh

Journal

Applied and Environmental Microbiology, 90(9)

Authors

Xu, Fengjun

Thoma, Calvin

Zhao, Weiyang

et al.

Publication Date

2024-09-18

DOI

10.1128/aem.00602-24

Peer reviewed

Dual feedback inhibition of ATP-dependent caffeate activation economizes ATP in caffeate-dependent electron bifurcation

Fengjun Xu,[1] Calvin J. Thoma,[2] Weiyang Zhao,[1] Yiwen Zhu,[1] Yujie Men,[1,3] Lawrence P. Wackett[2]

AUTHOR AFFILIATIONS See affiliation list on p. 11.

ABSTRACT The acetogen *Acetobacterium woodii* couples caffeate reduction with ferredoxin reduction and NADH oxidation via electron bifurcation, providing additional reduced ferredoxin for energy conservation and cell synthesis. Caffeate is first activated by an acyl-CoA synthetase (CarB), which ligates CoA to caffeate at the expense of ATP. After caffeoyl-CoA is reduced to hydrocaffeoyl-CoA, the CoA moiety in hydrocaffeoyl-CoA could be recycled for caffeoyl-CoA synthesis by an ATP-independent CoA transferase (CarA) to save energy. However, given that CarA and CarB are co-expressed, it was not well understood how ATP could be saved when both two competitive pathways of caffeate activation are present. Here, we reported a dual feedback inhibition of the CarB-mediated caffeate activation by the intermediate hydrocaffeoyl-CoA and the end-product hydrocaffeate. As the product of CarA, hydrocaffeate inhibited CarB-mediated caffeate activation by serving as another substrate of CarB with hydrocaffeoyl-CoA produced. It effectively competed with caffeate even at a concentration much lower than caffeate. Hydrocaffeoyl-CoA formed in this process can also inhibit CarB-mediated caffeate activation. Thus, the dual feedback inhibition of CarB, together with the faster kinetics of CarA, makes the ATP-independent CarA-mediated CoA loop the major route for caffeoyl-CoA synthesis, further saving ATP in the caffeate-dependent electron-bifurcating pathway. A genetic architecture similar to *carABC* has been found in other anaerobic bacteria, suggesting that the feedback inhibition of acyl-CoA ligases could be a widely employed strategy for ATP conservation in those pathways requiring substrate activation by CoA.

IMPORTANCE This study reports a dual feedback inhibition of caffeoyl-CoA synthetase by two downstream products, hydrocaffeate and hydrocaffeoyl-CoA. It elucidates how such dual feedback inhibition suppresses ATP-dependent caffeoyl-CoA synthesis, hence making the ATP-independent route the main pathway of caffeate activation. This newly discovered mechanism contributes to our current understanding of ATP conservation during the caffeate-dependent electron-bifurcating pathway in the ecologically important acetogen *Acetobacterium woodii*. Bioinformatic mining of microbial genomes revealed contiguous genes homologous to *carABC* within the genomes of other anaerobes from various environments, suggesting this mechanism may be widely used in other CoA-dependent electron-bifurcating pathways.

KEYWORDS *Acetobacterium woodii*, CarB, CarA, acetogen, caffeate reduction, feedback inhibition, energy conservation, flavin-based electron bifurcation

Acetogenic bacteria, such as the model acetogen *Acetobacterium woodii*, fix CO$_2$ through the well-known Wood–Ljungdahl pathway. As facultative autotrophs, they can also generate energy by oxidizing various organic substrates (1, 2). Acetogenic bacteria exhibit great metabolic diversity (3). Within the genomes of *Acetobacterium*, unique and diverse metabolic features have been identified (4), including caffeate

reduction coupled with a recently discovered mechanism known as flavin-based electron bifurcation (5, 6). Electron bifurcation is a biological process by which a redox cofactor, typically a flavin, dismutates the energy of an electron pair to raise the energy level of one at the expense of the other. To date, several electron-bifurcating enzyme systems in different bacteria have been discovered and characterized (7–18), including the caffeoyl-CoA reductase involved in caffeate reduction (9).

As a degradation product of lignin, caffeate is ubiquitous in nature and readily accessible to microbes as a potential electron acceptor. The caffeate-dependent electron-bifurcating pathway by *A. woodii* gives growth benefits to cells (19–21). When H_2 or fructose is provided, *A. woodii* can reduce caffeate to hydrocaffeate, an end-product that is not further metabolized (22).

In *A. woodii*, the genes involved in caffeate reduction have been identified (Fig. 1A) and are clustered in the *car* (caffeate reduction) operon (23). The encoded enzymes have been functionally characterized (Fig. 1B). An acyl-CoA ligase (CarB) initiates the reaction by ligating CoA to caffeate for caffeate activation at the expense of ATP (23). Once caffeoyl-CoA is reduced to hydrocaffeoyl-CoA by the CarCDE complex (9, 24), caffeate activation can be achieved by an ATP-independent CoA transferase (CarA), which recycles CoA from hydrocaffeoyl-CoA (25). The CarA-mediated CoA loop does not require ATP and is proposed to save energy in comparison to CarB-mediated ATP-dependent caffeate activation (23, 25). However, this CoA loop has not been demonstrated *in vitro*, and it was not well understood how CarA could outcompete CarB when they are both present given the coexpression of all *car* genes.

In this study, we aimed to elucidate whether and how the CoA loop mediated by CarA could be dominant in caffeoyl-CoA synthesis so as to save more energy. By heterologously expressing CarA and CarB, we conducted *in vitro* enzyme assays to identify potential inhibitors of the CarB-mediated ATP-dependent CoA synthesis pathway. We further used *in vitro* enzyme assay systems consisting of both CarA and CarB, as well as their substrates, to demonstrate how they work together to synthesize caffeoyl-CoA from caffeate in a more economical way. Lastly, a search of *carABC* homologs was carried out to indicate how common this genetic architecture is as an energy-saving strategy employed by other microorganisms in nature.

RESULTS

Hydrocaffeate inhibited CarB-catalyzed caffeoyl-CoA synthesis

To investigate how the end-product hydrocaffeate would affect caffeoyl-CoA synthesis (Fig. 2A), *carB* from *A. woodii* was heterologously expressed in *E. coli*, and the protein was purified. The effects of hydrocaffeate on the Michaelis–Menten curve of caffeate are shown in Fig. 2B and Table 1. Without hydrocaffeate, K_m and V_{max} were determined to be 14.6 µM and 92.4 mU/mg, respectively, similar to the values previously reported (23). In the presence of 0.05 mM caffeate, however, the K_m was increased to 68.9 µM, and the V_{max} was decreased to 64.8 mU/mg. When the concentration of hydrocaffeate was 0.1 and 0.2 mM, K_m was further increased, and V_{max} was decreased. Hydrocaffeate greatly inhibits CarB-mediated caffeoyl-CoA synthesis. The trend of K_m and V_{max} indicated a combination of competitive and noncompetitive inhibition.

The inhibition effect was also tested on two other substrates, ATP (Fig. 2C; Table 1) and CoA (Fig. 2D; Table 1). As hydrocaffeate concentration became higher, the V_{max} with ATP decreased from 82.3 to 21.9 mU/mg, and that with CoA decreased from 421 to 60 mU/mg. As more hydrocaffeate was added, the K_m of ATP increased from 16.0 to 53.7 µM, while the K_m of CoA decreased from 1,900 to 830 µM. These results further demonstrated hydrocaffeate inhibition on caffeoyl-CoA synthesis catalyzed by CarB.

Tryptophan fluorescence spectroscopy was applied to investigate protein–ligand interactions. Purified CarB exhibits significant fluorescence due to four tryptophan residues (Fig. S1). Substrate binding can cause conformational change and may increase or decrease fluorescence intensity. Purified CarB was titrated with caffeate and hydrocaffeate, both of which greatly decreased fluorescence intensity (Fig. 2E and F). The K_D of

TABLE 1 Calculated K_m and V_{max} of substrates with different hydrocaffeate concentrations

Substrate	Hydrocaffeate (mM)	K_m (µM)	V_{max} (mU/mg)
Caffeate	0	**14.6** (11.0–18.7)[a]	**92.4** (88.9–96.0)
	0.05	**68.9** (56.6–83.4)	**64.8** (91.0–69.1)
	0.10	**152** (121–192)	**42.1** (38.1–47.0)
	0.20	**112** (89.4–141)	**20.7** (19.0–22.7)
ATP	0	**16.0** (10.8–22.3)	**82.3** (77.7–87.1)
	0.05	**36.9** (28.2–47.5)	**58.3** (54.7–62.2)
	0.10	**54.8** (43.3–68.7)	**40.0** (37.4–42.9)
	0.20	**53.7** (38.2–74.1)	**21.9** (19.9–24.2)
CoA	0	**1,900** (1,680–2,150)	**421** (397–448)
	0.05	**1,210** (1,070–1,380)	**207** (196–218)
	0.10	**890** (862–1,150)	**120** (114–128)
	0.20	**830** (709–969)	**60.4** (57.1–63.9)

[a]The number in bold means the best-fit value, and the range corresponds to 95% confidence interval.

caffeate and hydrocaffeate was estimated to be 64 and 313 µM, respectively. The decrease in fluorescence intensity caused by caffeate or hydrocaffeate was different, suggesting distinct conformational changes. We also titrated purified CarB with ATP, CoA, and AMP, all of which did not cause any significant change in fluorescence intensity (Fig. S2). This indicated that only caffeate and hydrocaffeate can bind to the resting state of the enzyme.

Hydrocaffeoyl-CoA serves as another CarB inhibitor

To examine how the two caffeoyl-CoA synthetic routes (CarB vs CarA) compete with each other, we conducted a combined *in vitro* assay containing CarA and CarB and all reactants required for CarA (0.5 mM caffeate and 0.14 mM hydrocaffeoyl-CoA) and CarB (0.5 mM caffeate, 1.86 mM CoA, and 1.86 mM ATP), as well as the newly identified inhibitor hydrocaffeate (0.06 mM). Hydrocaffeoyl-CoA was synthesized using a 4-coumarate:CoA ligase with 0.5 mM hydrocaffeate, 5 mM CoA, and 5 mM ATP. After 2 h, 70% hydrocaffeate was converted to hydrocaffeoyl-CoA (Fig. S3 and S4). For the combined *in vitro* assay, we also set up three groups using the same reactants but (i) without enzyme, (ii) with CarA only, and (iii) with CarB only. For CarA only, almost all hydrocaffeoyl-CoA was converted to caffeoyl-CoA after 20 min, and caffeoyl-CoA formation ceased due to the near depletion of hydrocaffeoyl-CoA (Fig. 3; Fig. S5). For CarB only, minor caffeoyl-CoA formation was observed due to hydrocaffeate inhibition.
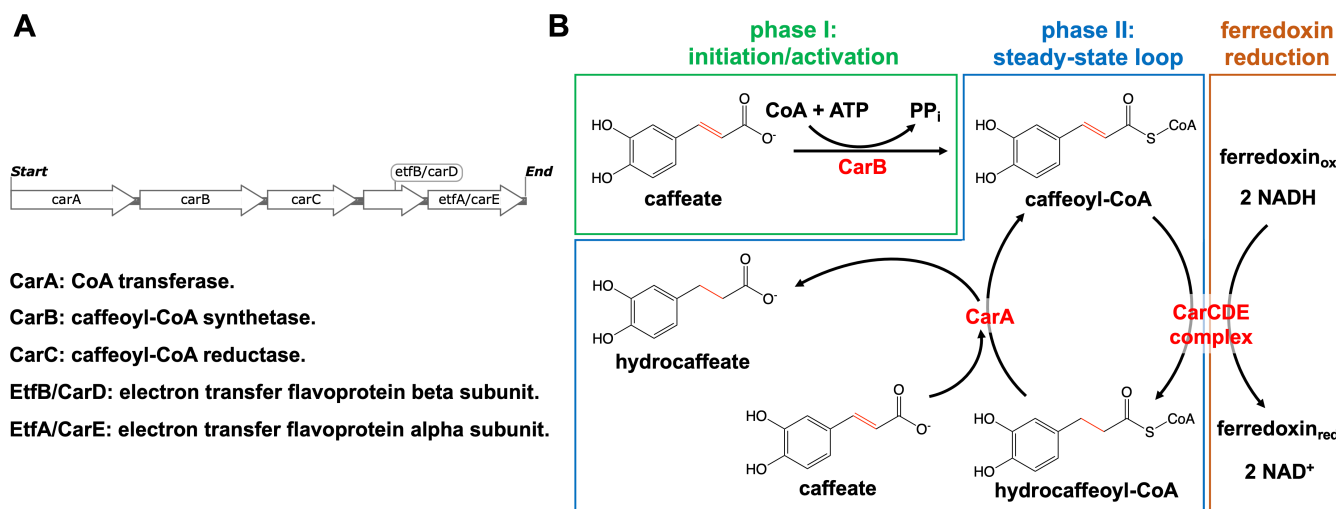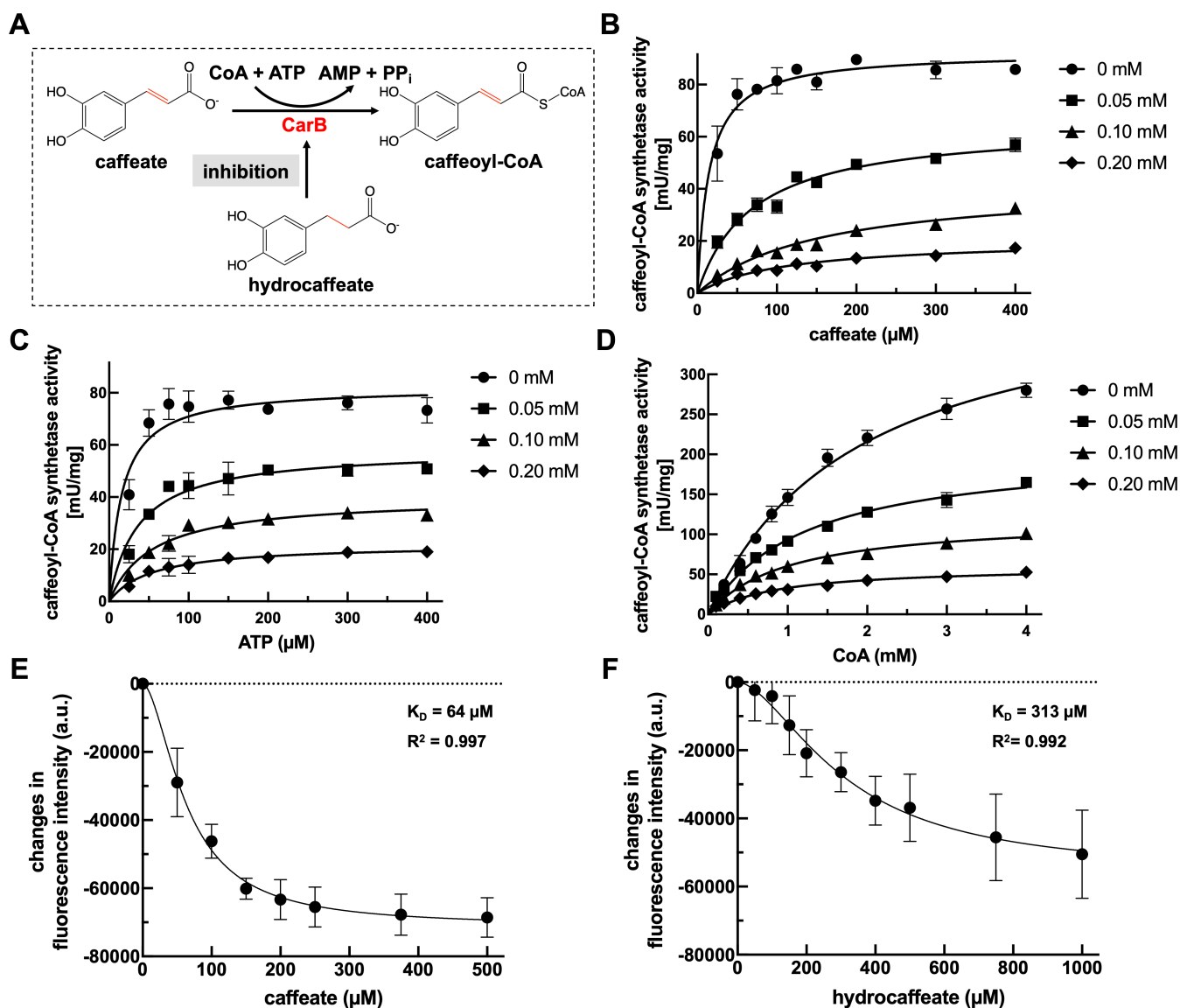

FIG 1 (A) The *car* operon and (B) the caffeate reduction pathway in *A. woodii*.

FIG 2 Hydrocaffeate inhibits CarB-mediated caffeoyl-CoA synthesis. (A) Illustration of the caffeoyl-CoA synthesis reaction catalyzed by CarB and inhibited by hydrocaffeate. Michaelis–Menten kinetics of (B) caffeate, (C) ATP, and (D) CoA influenced by different hydrocaffeate concentrations (0.05, 0.10, and 0.20 mM). All reactions were carried out in the same system with the same concentrations (0.5 mM caffeate, 1.0 mM ATP, and 0.5 mM CoA) except the carrying reactant. Two micrograms of CarB was added to initiate reactions. Data are presented as the mean ± SD ($n = 4$). Changes in fluorescence intensity of CarB (1 µM) solution titrated with (E) caffeate and (F) hydrocaffeate. Data are presented as the mean ± SD ($n = 3$).

Surprisingly, hydrocaffeate was depleted in tandem with hydrocaffeoyl-CoA formation (Fig. 3B), indicating that hydrocaffeate is a substrate of CarB as well and can be CoA-activated the same as caffeate. Moreover, although the inhibition of hydrocaffeate was removed after all hydrocaffeate was converted to hydrocaffeoyl-CoA, there was still very minor caffeoyl-CoA synthesis (47 µM) compared to the normal condition without inhibition (149 µM) (Fig. S6). This implied that the intermediate hydrocaffeoyl-CoA also inhibited CarB and repressed the ATP-dependent caffeoyl-CoA synthesis. Due to the challenges in getting rid of hydrocaffeate residues in the synthesized hydrocaffeoyl-CoA via our method, the binding properties and inhibition mechanism of hydrocaffeoyl-CoA on CarB remain unclear and warrant further investigation when highly pure hydrocaffeoyl-CoA becomes available.

When both CarA and CarB were added, the caffeoyl-CoA formation was much higher than that in the CarA-only condition, whereas the concentration of hydrocaffeate and
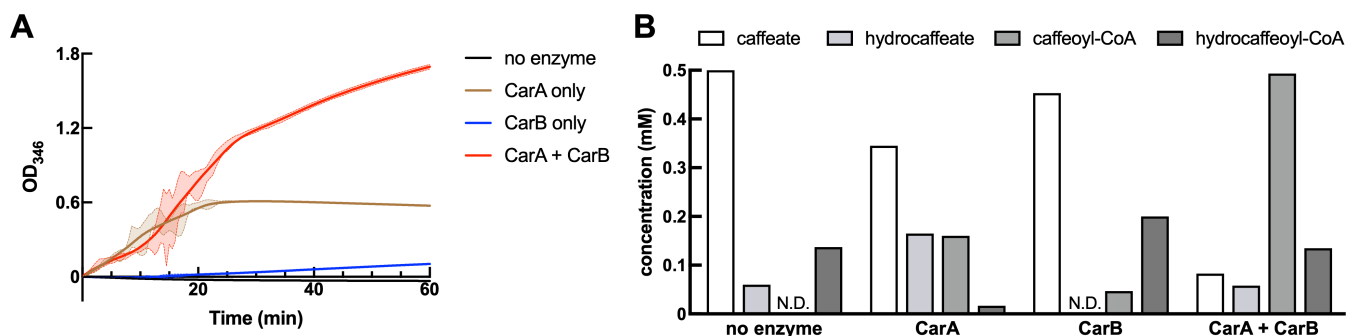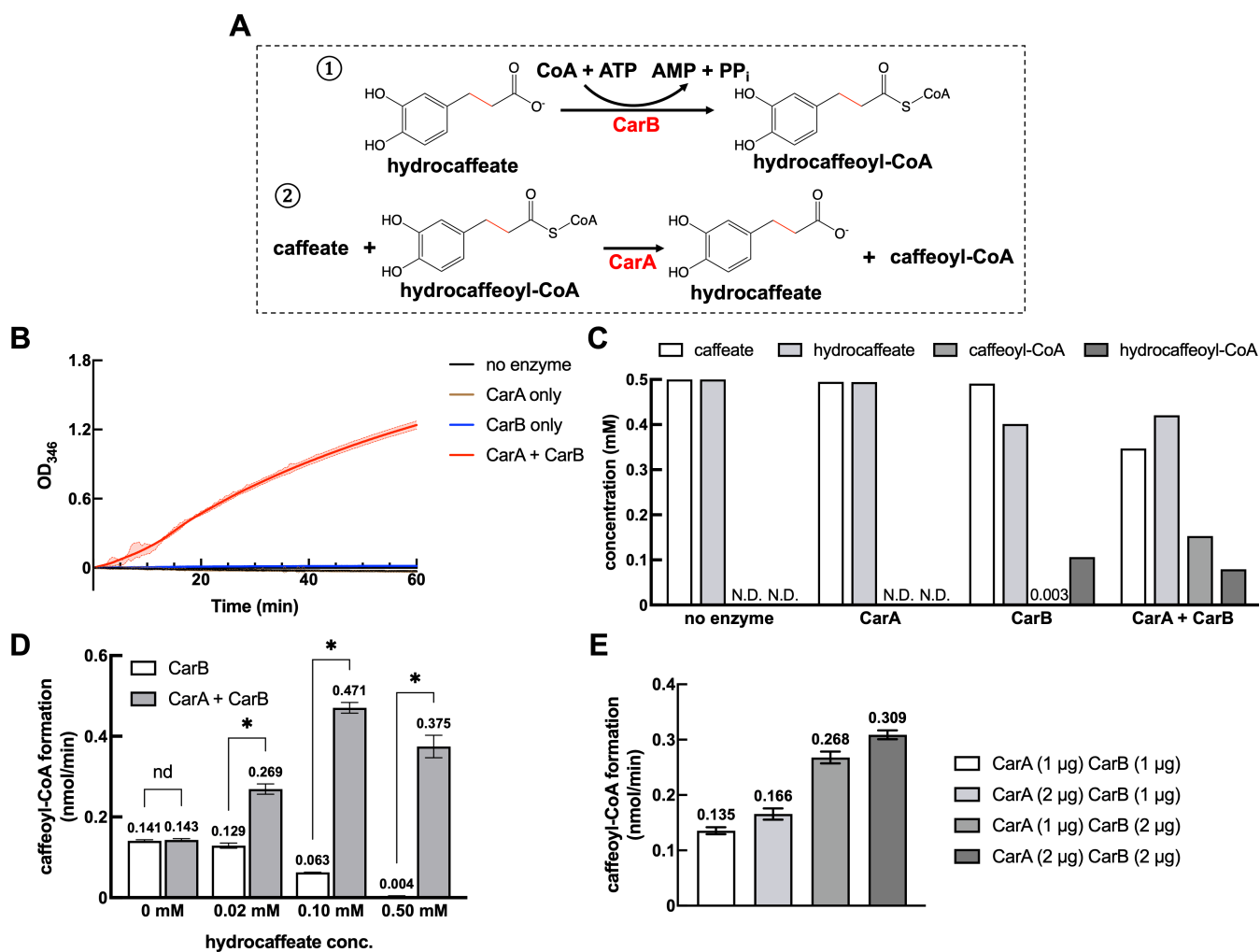
FIG 3 Caffeoyl-CoA synthesis in separate or combined *in vitro* enzyme systems. (A) Caffeoyl-CoA formation with either CarA, CarB, or both. Each 200-µL reaction system contains 0.5 mM caffeate, 0.06 mM hydrocaffeate, 0.14 mM hydrocaffeoyl-CoA, 1.86 mM ATP, and 1.86 mM CoA. Two micrograms of CarA and CarB was used. Solid lines represent the fitting curves of the mean of caffeoyl-CoA formation, and dashed lines of the same color represent the standard deviation ($n = 4$). (B) Concentrations of reactants and products after a 1-h reaction (all four reactants and products were quantified or semi-quantified by high-performance liquid chromatography equipped with UV/Vis detector (HPLC-UV/Vis), except for hydrocaffeoyl-CoA, the concentration of which was back-calculated based on the mass balance of the corresponding reactant/product, hydrocaffeate. N.D., not detected).

hydrocaffeoyl-CoA did not change. Given the CarB activity of caffeoyl-CoA synthesis was significantly inhibited, the additional caffeoyl-CoA production must come from the CarA-mediated CoA transfer reaction. The amount of initially added hydrocaffeoyl-CoA was not enough to form the observed high yield of caffeoyl-CoA. Therefore, additional hydrocaffeoyl-CoA was made available to CarA, most likely from the activity of CarB to hydrocaffeate. Based on this, we proposed a looped caffeoyl-CoA synthetic pathway to explain the continuous caffeoyl-CoA formation in the CarA and CarB combined systems (Fig. 4A). First, CarB ligates CoA to hydrocaffeate to form hydrocaffeoyl-CoA. Then, CarA transfers CoA from hydrocaffeoyl-CoA to caffeate, resulting in the additional caffeoyl-CoA formation compared to the CarA-only system and the release of hydrocaffeate. The overall reaction is ligating CoA to caffeate and producing caffeoyl-CoA, which is consistent with no changes in hydrocaffeate and hydrocaffeoyl-CoA concentrations (Fig. 3B).

CarA and CarB work together for energy-efficient caffeoyl-CoA synthesis

The above results suggest that hydrocaffeate could not only suppress CarB-mediated caffeoyl-CoA formation but also help initiate the CarA-mediated CoA loop by being activated to hydrocaffeoyl-CoA by CarB. We further demonstrate this by CarA (2 µg) and CarB (2 µg) combined systems containing caffeate (0.5 mM), hydrocaffeate (0.02–0.5 mM), CoA (0.5 mM), and ATP (1 mM), with CarA only or CarB only as controls. As expected, only when both CarA and CarB were added would caffeoyl-CoA be produced significantly (Fig. 4B and C; Fig. S7). Hydrocaffeate was converted to hydrocaffeoyl-CoA by CarB, followed by CoA transfer from hydrocaffeoyl-CoA to caffeoyl-CoA mediated by CarA. In comparison, for CarA only, no enzyme activities were detected because no hydrocaffeoyl-CoA was provided. For CarB only, hydrocaffeate was consumed with hydrocaffeoyl-CoA produced, and very minor caffeoyl-CoA was detected, corroborating the dual feedback inhibition on CarB-mediated caffeate activation. These results provided strong evidence for the proposed energy-efficient caffeoyl-CoA synthesis initiated by ATP-dependent CarB reaction and sustained by ATP-independent CarA reaction.

Given that hydrocaffeate and hydrocaffeoyl-CoA can be recycled and both effectively inhibit CarB-mediated caffeate activation, it is expected that only a small amount of hydrocaffeate would be enough to sustain the caffeoyl-CoA formation from the CarA-mediated CoA loop. We, therefore, tested different hydrocaffeate concentrations to see how much hydrocaffeate is needed for efficient caffeoyl-CoA synthesis (Fig. 4D). In comparison to the pathway catalyzed by CarB alone, with 0.02 mM hydrocaffeate (25 times lower than caffeate), the presence of CarA increased caffeoyl-CoA formation from 0.129 to 0.269 nmol/min, i.e., half of caffeoyl-CoA was from the CoA loop. Caffeoyl-CoA

FIG 4 Looped caffeoyl-CoA synthetic pathway starting from hydrocaffeate and catalyzed by both CarA and CarB. (A) Caffeoyl-CoA synthesis initiated by CarB-mediated hydrocaffeate activation and followed by CarA-mediated CoA transfer. (B) Caffeoyl-CoA formation with either CarA, CarB, or both. Each 200-μL reaction system contains 0.5 mM caffeate, 0.5 mM hydrocaffeate, 1 mM ATP, and 0.5 mM CoA. Two micrograms of CarA and CarB was used. Solid lines stand for the fitting curves of the mean of caffeoyl-CoA formation, and dashed curves of the same color represent the standard deviation ($n = 4$). (C) Concentrations of reactants and products after a 1-h reaction (all four reactants and products were quantified or semi-quantified by HPLC-UV/Vis, except for hydrocaffeoyl-CoA, the concentration of which was back-calculated based on the mass balance of the corresponding reactant, hydrocaffeate. (D) Caffeoyl-CoA formation determined in the same enzymatic systems as (B) but with varying hydrocaffeate concentrations. Multiple unpaired t-tests were performed for statistical analysis. nd, not a discovery. $^*P < 0.01$. (E) Caffeoyl-CoA formation determined in the same enzymatic systems as (B) but with varying CarA or CarB concentrations. All data are presented as the mean ± SD ($n = 4$).

synthesis directly from CarB was inhibited by ~10% compared to no hydrocaffeate addition. With 0.10-mM hydrocaffeate (five times lower than caffeate), a much higher caffeoyl-CoA production was observed, which was mainly attributed to the CoA loop, whereas the direct synthesis by CarB was inhibited by more than half. When hydrocaffeate reached 0.5 mM (equal to caffeate), the direct synthesis by CarB was almost completely inhibited, and nearly all caffeoyl-CoA formation was from the looped pathway. Since the caffeate concentration used in all groups was 0.5 mM, it is worth noting that the looped caffeoyl-CoA synthetic pathway is dominant even when the concentration of hydrocaffeate is much lower than that of caffeate.

Because the looped caffeoyl-CoA synthetic pathway requires both CarA and CarB, we tested which reaction is the rate-limiting one by reducing enzyme concentrations (Fig. 4E). When the amount of CarB was lowered by half, the caffeoyl-CoA formation rate was decreased by half as well. In contrast, lowering the amount of CarA only slightly

decreased caffeoyl-CoA formation. Given the similar molarity of CarA (56.2 kDa) and CarB (58.8 kDa), CarA is more efficient than CarB in this process. The first reaction catalyzed by CarB is the rate-limiting step. This implied faster kinetics of CarA than that of CarB, which is consistent with the k_{cat} values of CarA and CarB previously reported (23, 25).

DISCUSSION

The previously unknown dual feedback inhibition by hydrocaffeate and hydrocaffeoyl-CoA serves to block the ATP-dependent CarB-mediated caffeate activation (Fig. 5). Thus, it facilitates the more energy-efficient CarA-mediated CoA loop, together with the previously reported faster turnover of caffeate by CarA than CarB (23, 25). The mechanism of the inhibition by hydrocaffeate and hydrocaffeoyl-CoA was different. How much the two inhibitors contribute to inhibition depends on their dynamic concentrations in cells. Hydrocaffeate is the output product of caffeate reduction (19, 26). An *in vivo* test showed that the extracellular concentration of caffeate and hydrocaffeate maintained a good mass balance (100%) during caffeate metabolism (Fig. S8), indicating that *A. woodii* can efficiently export hydrocaffeate out of cells as soon as it is generated. Meanwhile, even at concentrations as low as 0.02 mM, hydrocaffeate could still exhibit 10% inhibition on CarB-mediated caffeate activation (Fig. 4D). Collectively, the intracellular hydrocaffeate, if any, seems to remain at low concentration levels and may only slightly inhibit CarB-mediated caffeoyl-CoA synthesis. Therefore, intracellular intermediate hydrocaffeoyl-CoA is more likely the primary inhibitor *in vivo*, although it is difficult to estimate its dynamic concentration which depends on the enzyme kinetics of caffeoyl-CoA reduction by the CarCDE complex. Because hydrocaffeoyl-CoA is formed from caffeoyl-CoA reduction *in vivo*, inhibiting the CarB-mediated caffeate activation route by hydrocaffeoyl-CoA would be more economical than by hydrocaffeate, which still costs one ATP for activation when competing CarB with caffeate.

CarB is a member of the ANL superfamily that includes CoA-synthetases/ligases (27, 28), of which aromatic CoA ligases are a significant subfamily (29). Feedback inhibition for regulating activities has been reported in various acyl-CoA ligases, but the mechanisms and the purposes can be quite different. A microsomal long-chain acyl-CoA ligase is inhibited by palmityl-CoA, which will compete with the substrate CoA, and the competitive inhibition can be reversed by providing excessive CoA (30). In the monolignol biosynthesis of *Populus trichocarpa*, the 4-coumaroyl-CoA/caffeoyl-CoA ligase is inhibited by the intermediates 4-coumaroyl/caffeoyl shikimic acids via competitive and noncompetitive inhibition (31, 32). A tomato peel 4-coumaroyl-CoA ligase is strongly inhibited by naringenin, a downstream product of the pathway, via allosteric inhibition (33). In Lin et al. (31, 32), the metabolic logic is to provide feedback inhibition for intermediate buildup during the biosynthesis of structural polymers. The regulation described here has a different metabolic purpose, functioning to conserve energy in anaerobic bacteria that may operate near thermodynamic limits of energy conservation, such as *Acetobacterium* spp. (1).

The energy-saving loop maintained by CarA can be found in other anaerobic metabolic pathways. For example, energy is saved in this similar mode during toluene catabolism in *Thauera aromatica* (34) or during the first step of oxalate degradation in *Oxalobacter formigenes* (35). It was previously discussed that other bacteria have a similar constellation of genes as the *car* operon in *A. woodii* (25), specifically *Pelosinus fermentans* and *Holophaga foetida*. Here, we extended this idea using the Rapid ORF Description and Evaluation Online (RODEO) tool to search for contiguous genes homologous to *carABC*, as described in Materials and Methods (Table S2). In the table, the identified top genera are *Acetobacterium*, *Lachnoclostridium*, *Clostridium*, *Enterocloster*, *Youngibacter*, *Flavonifractor*, *Lacrinispora*, and *Murimona*, all of which possessed specific gene regions with continuous *carABC* homologs (Fig. 6). The *e*-values presented derive from a protein BLAST alignment between each translated gene and the corresponding translated gene from *Acetobacterium woodii*. Generally, *e*-values of *e*−5 or lower are considered highly likely to be members of the same protein family (36), and sequence similarity networks
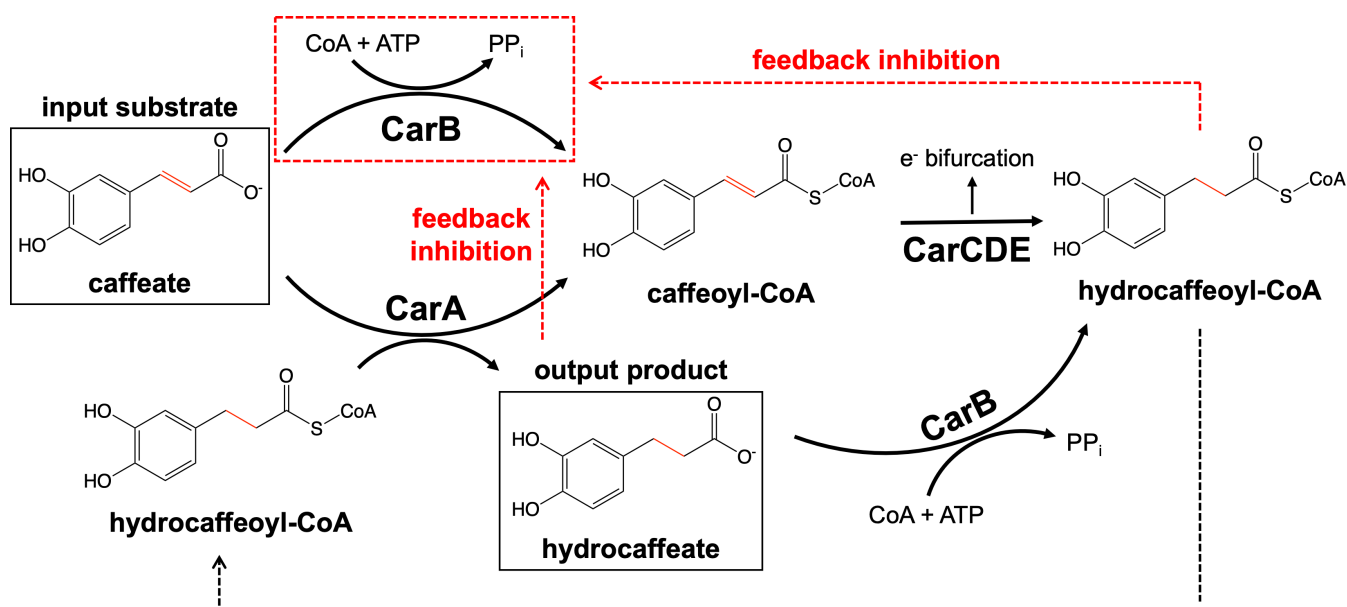
FIG 5 A modified caffeate reduction pathway including the dual feedback inhibition of CarB-mediated caffeate activation.

typically associate proteins with the same function in the $e-20$ to $e-40$ range (37). The average e-values for homologs to CarA, CarB, and CarC shown in Fig. 6 are $e-37$, $e-74$, and $e-53$, respectively. Additionally, in several of the genera listed, electron-bifurcating dehydrogenases have been reported to react with short-chain CoA esters (7, 8, 38, 39). Given the widespread distribution of these genera in various environments (Fig. 6) (4, 40–45), the feedback inhibition to slow or halt the activity of acyl-CoA ligases may be a widely employed strategy in different biological contexts for saving ATP.

MATERIALS AND METHODS

Gene cloning

The genes *carA* and *carB* were amplified from the chromosome of *A. woodii* DSM1030 using PCR. The gene, which encodes a 4-coumarate:CoA ligase (PDB entry ID: 3A9U_A), was codon-optimized and synthesized by Twist Bioscience. The primers used for cloning are listed in Table S1. A 6×His tag was fused into the C-terminal for protein purification. PCR was performed using Takara PrimeSTAR Max DNA Polymerase. The overexpression plasmid pET28a (Addgene: #85492) was digested with restriction enzymes NcoI/XhoI and purified by gel extraction. Purified PCR products were ligated to the linearized pET28a backbone by Takara In-Fusion Snap Assembly cloning kits, under the manufacturer's instructions. The mixture was transformed into chemically competent *E. coli* DH5α. After growing overnight, transformants on kanamycin selection plates were picked and screened. Gene integrity was verified by Sanger sequencing.

Protein production and purification

The recombinant plasmid was transformed into chemically competent *E. coli* BL21 (DE3). Transformants were picked and screened the same as *E. coli* DH5α mentioned above. After successful transformation, a single colony was inoculated into 20 mL of Luria-Bertani (LB) medium with 50 µg/mL kanamycin and grown overnight at 180 rpm and 37°C. Overnight culture was inoculated into 1 L of LB medium with 50 µg/mL kanamycin and grown at 180 rpm and 37°C. When the optical density at 600 nm (OD_{600}) reached 0.6–0.8, isopropyl β-D-1-thiogalactopyranoside was added to 1 mM in media. Cells were cultured overnight at 180 rpm and 16°C and harvested by centrifugation (6,000 × *g*,

Genus	Environment or characteristic feature	Representative accession ID	Gene region	e-value of carA	e-value of carB	e-value of carC
Acetobacterium	Widespread (4)	WP_186842988.1		3.4e-35	1.8e-84	9.4e-57
Lachnoclostridium	Human gut (40)	WP_227809101.1		1.1e-29	1.9e-70	1.3e-48
Clostridium	Widespread (41)	WP_103229327.1		5.7e-38	1.6e-92	2.9e-55
Enterocloster	Human or animal feces (42)	WP_048929254.1		6.0e-31	4.5e-70	6.9e-49
Youngiibacter	Gas-production water (43)	WP_023384640.1		1.3e-30 1.4e-35	5.0e-82	1.6e-56
Flavonifractor	Human gut (44)	WP_186907497.1		9.8e-38	1.8e-14	2.9e-52
Lacrimispora	Human gut (42)	WP_227148893.1		2.1e-29	6.5e-93	1.0e-55
Murimonas	Mammalian intestine (45)	WP_109625135.1		7.7e-39	2.3e-97	1.4e-54

FIG 6 Screened contiguous homologs to *carA*, *carB,* and *carC* of *A. woodii* in the database. The RODEO tool was probed to find the bacterial genera showing contiguous *carABC* homologs using seed sequences. The homologs are designated by arrows to the following genes (colors): *carA* (red), *carB* (green), and *carC* (blue). The *e*-values were generated from RODEO and described further in Materials and Methods.

10 min, 4°C). Pellets were frozen at −80°C for 24 h and resuspended in buffer A (50 mM NaH$_2$PO$_4$, 300 mM NaCl, pH 7). After the resuspension, cells were lysed by passing through a French pressure cell press at 1,000 p.s.i. three times. Following centrifugation at 18,000 × *g* for 1.5 h, supernatants were loaded onto a GE Healthcare ÄKTA fast protein liquid chromatography system equipped with a HisTrap HP 5 mL Ni^{2+} column. Proteins were washed and eluted with gradients of buffer A and 250 mM imidazole. Protein purity was tested by 12.5% SDS-PAGE. Purified proteins were equilibrated into buffer B [20 mM 2-[4-(2-hydroxyethyl)piperazin-1-yl]ethanesulfonic acid (HEPES), 200 mM NaCl, pH 7] using Amicon Ultra 30-kDa centrifugal units. Protein concentration was determined by the Bradford assay using the Protein Assay Dye Reagent (Bio-Rad).

CarB activity inhibited by hydrocaffeate

The inhibition test of CarB-catalyzed caffeoyl-CoA synthesis by hydrocaffeate was modified from one previous CarB enzyme assay (23). The test was done in clear 96-well microplates at 30°C. Caffeoyl-CoA formation was monitored to evaluate enzyme activities as mentioned in Analytical Methods. The buffer was made up of 50 mM morpholineethanesulfonic acid (MES), 50 mM Tris, 25 mM KCl, and 5 mM MgCl$_2$ (pH 7). Caffeate, CoA, ATP, and hydrocaffeate were added individually. For the Michaelis–Menten kinetics of caffeate, the reaction consists of caffeate (25–400 µM), 0.5 mM CoA, 1.0 mM ATP, and hydrocaffeate (0, 0.05, 0.1, and 0.2 mM). For CoA, the reaction consists of 0.5 mM caffeate, CoA (0.1–4.0 mM), 1.0 mM ATP, and hydrocaffeate (0, 0.05, 0.1, and 0.2 mM). For ATP, the reaction consists of 0.5 mM caffeate, 0.5 mM CoA, ATP (25–400 µM), and hydrocaffeate (0, 0.05, 0.1, and 0.2 mM). Two micrograms of CarB was added at the end to initiate the reaction. Each reaction took 20 min. Four replicates were set for each group. Nonlinear fitting of Michaelis–Menten kinetics "$V = V_{max} \times [S]/(K_m + [S])$" was performed in GraphPad Prism v10.0.0 with default settings.

Tryptophan fluorescence spectroscopy

Tryptophan fluorescence spectroscopy was performed using the Synergy H1M Microplate Reader (BioTek) and black/clear bottom 96-well microplates. All reagents were dissolved in buffer B (20 mM HEPES, 200 mM NaCl, pH 7). CarB (1 µM) solution was titrated with caffeate, hydrocaffeate, ATP, CoA, and AMP, respectively. The excitation wavelength was fixed to 280 nm, and the emission wavelength was set to 335 nm. The temperature was maintained constant at room temperature (20°C–22°C). The blank control (buffer titration) without CarB was performed to determine the background level, which was subtracted to get the fluorescence signal from CarB. Three replicates were set for all experiments. Nonlinear regression analysis of specific binding with hill slope "$Y = B_{max} \times X^h/(K_D^h + X^h)$" was performed in GraphPad Prism v10.0.0 with default settings.

Hydrocaffeoyl-CoA synthesis

Hydrocaffeoyl-CoA was synthesized using the purified 4-coumarate:CoA ligase. The reaction was performed at 30°C in 1.5-mL tubes. The buffer was prepared according to one previous enzymatic assay (46), with minor modifications. Briefly, the 500-μL system consists of 0.5 mM hydrocaffeate, 5 mM CoA, 5 mM ATP, 5 mM $MgCl_2$, and 0.2 M Tris-HCl (pH 7.5). The reaction was initiated by adding 80 μg of purified proteins. After 2 h, proteins were removed using 10 kDa VWR centrifugal filters. After centrifugating at $6,000 \times g$ for 30 min, filtrate was collected and stored at 4°C for downstream analysis and experiments. To verify hydrocaffeoyl-CoA formation, high-performance liquid chromatography equipped with UV/Vis detector (HPLC-UV/Vis) and ultrahigh-performance liquid chromatography coupled to high-resolution tandem mass spectrometry (UHPLC-HRMS/MS) were applied, as mentioned in Analytical Methods.

Caffeoyl-CoA synthesis by CarA and CarB combined systems

The buffer was made up of 50 mM MES, 50 mM Tris, 25 mM KCl, and 5 mM $MgCl_2$ (pH 7). The reaction consists of 0.5 mM caffeate, 0.06 mM hydrocaffeate, 0.14 mM hydrocaffeoyl-CoA, 1.86 mM CoA, and 1.86 mM ATP. Hydrocaffeate, hydrocaffeoyl-CoA, CoA, and ATP came from the mixture of hydrocaffeoyl-CoA synthesis, and concentrations were estimated based on 70% conversion of hydrocaffeate to hydrocaffeoyl-CoA. Four groups were included: (i) the negative control with no enzyme, (ii) the group with CarA, (iii) the group with CarB, and (iv) the group with both CarA and CarB. Caffeoyl-CoA formation was monitored the same as that in CarB Activity Inhibited by Hydrocaffeate for 60 min. CarA (2 μg) and/or CarB (2 μg) were added. Four replicates were set for each group. Smooth curves of caffeoyl-CoA synthesis were obtained by Fit LOWESS in GraphPad Prism v10.0. After a 1-h reaction, 10 μL of samples was injected into the HPLC-UV/Vis system as mentioned in Analytical Methods. For the verification test of the CoA loop caffeoyl-CoA synthesis, all experimental setups were the same as the above, except the components. The reaction consists of 0.5 mM caffeate, 0.5 mM hydrocaffeate, 0.5 mM CoA, and 1 mM ATP. Hydrocaffeate titration and CarA/CarB titration were tested under the same conditions. Four replicates were set for each group.

Caffeate reduction by *Acetobacterium woodii* cells

A. woodii DSM 1030 was grown anaerobically in *Acetobacterium* medium 135 recommended by DSMZ. Pre-grown cells [$OD_{600} \approx 1.0$, 2% (vol/vol)] were inoculated into fresh media to initiate cell growth and caffeate reduction at 30°C without shaking. Caffeate was added from an anaerobically prepared 100 mM caffeate stock. Collected samples were centrifuged at $6,000 \times g$ for 15 min. Supernatants were collected and passed through a 0.22 μm filter. Ten microliters of filtrate was injected into a HPLC-UV/Vis system for analysis. Caffeate and hydrocaffeate were measured using HPLC-UV/Vis as described in Analytical Methods. Standard curves were generated and plotted for quantification.

Analytical methods

A Shimadzu HPLC-UV/Vis system was used to detect caffeate, hydrocaffeate, caffeoyl-CoA, and hydrocaffeoyl-CoA. The system consists of two LC-20AD-XR pumps, a CMB20A system controller, a Nexera-SIL-40XR autosampler, a UV/Vis SPD-M20A detector, and a CTD-10A controller. For the HPLC-UV/Vis analysis, 10 μL of the sample was injected into a ZORBAX Eclipse Plus C18 column (particle size 5 μm, 4.6×250 mm, Agilent) and eluted with 90% buffer (100 mM NaH_2PO_4, 75 mM $C_2H_3NaO_2$, pH 4.6) and 10% acetonitrile at 500 μL/min for 25 min.

Caffeate and hydrocaffeate were quantified on the HPLC-UV/vis using their reference compounds with a limit of quantification of <31.25 μM. Due to the lack of a reference compound, a semi-quantification was done on HPLC-UV/Vis for caffeoyl-CoA by correlating the peak area to the concentration calculated using the absorbance at 346 nm on a spectrophotometer (Synergy HYX Multimode Reader, BioTek) and the

extinction coefficient ε = 18 mM^{-1}·cm^{-1} (47). Due to the lack of reference compound and the overlapping absorbance at a wavelength <300 nm (Fig. S9) with ATP and CoA, it was unable to experimentally quantify hydrocaffeoyl-CoA, the concentration of which was, instead, back-calculated based on the mass balance of the reactant/product, hydrocaffeate.

A UHPLC-HRMS/MS (Thermo Fisher Scientific) was used to confirm the formation of hydrocaffeoyl-CoA during hydrocaffeoyl-CoA synthesis. The system consists of a Vanquish UHPLC system and a Q Exactive Orbitrap Mass Spectrometer. For UHPLC-HRMS/MS analysis, 2 µL of the sample was injected into a Hypersil GOLD column (particle size 1.9 µm, 100 × 2.1 mm, Thermo Fisher Scientific) and eluted with water (buffer A) and methanol (buffer B) at 300 µL/min. Both buffers were amended with 10 mM ammonium acetate. The gradient program was set as the following: 95% A: 0–1 min; 95%–5% A; 1–6 min; 5% A: 6–8.75 min; 95% A: 8.75–12 min. Mass spectra were acquired in the full scan mode at a resolution of 70,000 at m/z 200 and a scan range of m/z 70–1,050, in the negative mode of electrospray ionization. Xcalibur and FreeStyle (Thermo Fisher Scientific) were used for data acquisition and data analysis.

Gene cluster screening

To understand the dual feedback inhibition that could occur in other microbes, a list of 500 proteins with remote homology to CarC from *A. woodii* was identified using PSI-BLAST (48). The Refseq database was used to ensure the quality of associated assembly and taxonomic data. Briefly, CarC from *A. woodii* was used as a seed sequence, and 250 sequences were initially retrieved. After the initial search, five iterations of the search were conducted. To encompass a larger set of data, the search was expanded in a final iteration retrieving 500 sequences. Gene context data were retrieved using RODEO through their online webtool (2.0) (49). RODEO output data files were provided as Tables S3 and S4. Data were imported into RStudio (R language version 4.3.1), and gene windows were visualized using GenoPlotR (50). Homologs to *carA*, *carB*, and *carC* were highlighted with different colors in the gene windows. RODEO also generates *e*-values for the similarity to PFAMs through a Hidden Markov Model search. These *e*-values represent the likelihood that a particular protein is annotated by chance, meaning a lower *e*-value is more statistically relevant. The *e*-values for matching PF01144 (*carA*), PF00501 (*carB*), and PF00441 (*carC*) are displayed in the table.

AUTHOR AFFILIATIONS

[1]Department of Chemical and Environmental Engineering, University of California, Riverside, California, USA
[2]Department of Biochemistry, Molecular Biology & Biophysics, BioTechnology Institute, University of Minnesota, St. Paul, Minnesota, USA

3Department of Civil and Environmental Engineering, University of Illinois at Urbana-Champaign, Urbana, Illinois, USA

AUTHOR ORCIDs

Fengjun Xu ⓘ http://orcid.org/0000-0002-6627-2610
Yujie Men ⓘ http://orcid.org/0000-0001-9811-3828
Lawrence P. Wackett ⓘ http://orcid.org/0000-0002-3255-1101

ADDITIONAL FILES

The following material is available online.

Supplemental Material

Supplemental material (AEM00602-24-S0001.docx). Table S1; Figures S1 to S9.
Table S2 (AEM00602-24-S0002.pdf). Full screening results.
Table S3 (AEM00602-24-S0003.csv). Main co-occurrence results from RODEO.
Table S4 (AEM00602-24-S0004.csv). Main results from RODEO.

REFERENCES

1. Schuchmann K, Müller V. 2014. Autotrophy at the thermodynamic limit of life: a model for energy conservation in acetogenic bacteria. Nat Rev Microbiol 12:809–821. https://doi.org/10.1038/nrmicro3365
2. Schuchmann K, Müller V. 2016. Energetics and application of heterotrophy in acetogenic bacteria. Appl Environ Microbiol 82:4056–4069. https://doi.org/10.1128/AEM.00882-16
3. Müller V. 2003. Energy conservation in acetogenic bacteria. Appl Environ Microbiol 69:6345–6353. https://doi.org/10.1128/AEM.69.11.6345-6353.2003
4. Ross DE, Marshall CW, Gulliver D, May HD, Norman RS. 2020. Defining genomic and predicted metabolic features of the *Acetobacterium* genus. mSystems 5:e00277-20. https://doi.org/10.1128/mSystems.00277-20
5. Müller V, Chowdhury NP, Basen M. 2018. Electron bifurcation: a long-hidden energy-coupling mechanism. Annu Rev Microbiol 72:331–353. https://doi.org/10.1146/annurev-micro-090816-093440
6. Buckel W, Thauer RK. 2018. Flavin-based electron bifurcation, ferredoxin, flavodoxin, and anaerobic respiration with protons (ech) or NAD+ (Rnf) as electron acceptors: a historical review. Front Microbiol 9:401. https://doi.org/10.3389/fmicb.2018.00401
7. Herrmann G, Jayamani E, Mai G, Buckel W. 2008. Energy conservation via electron-transferring flavoprotein in anaerobic bacteria. J Bacteriol 190:784–791. https://doi.org/10.1128/JB.01422-07
8. Li F, Hinderberger J, Seedorf H, Zhang J, Buckel W, Thauer RK. 2008. Coupled ferredoxin and crotonyl coenzyme a (CoA) reduction with NADH catalyzed by the butyryl-CoA dehydrogenase/Etf complex from *Clostridium kluyveri*. J Bacteriol 190:843–850. https://doi.org/10.1128/JB.01417-07
9. Bertsch J, Parthasarathy A, Buckel W, Müller V. 2013. An electron-bifurcating caffeyl-CoA reductase. J Biol Chem 288:11304–11311. https://doi.org/10.1074/jbc.M112.444919
10. Schuchmann K, Müller V. 2012. A bacterial electron-bifurcating hydrogenase. J Biol Chem 287:31165–31171. https://doi.org/10.1074/jbc.M112.395038
11. Schut GJ, Adams MWW. 2009. The iron-hydrogenase of thermotoga maritima utilizes ferredoxin and NADH synergistically: a new perspective on anaerobic hydrogen production. J Bacteriol 191:4451–4457. https://doi.org/10.1128/JB.01582-08
12. Wang S, Huang H, Kahnt J, Mueller AP, Köpke M, Thauer RK. 2013. NADP-specific electron-bifurcating [FeFe]-hydrogenase in a functional complex with formate dehydrogenase in *Clostridium autoethanogenum* grown on CO. J Bacteriol 195:4373–4386. https://doi.org/10.1128/JB.00678-13
13. Wang S, Huang H, Kahnt J, Thauer RK. 2013. A reversible electron-bifurcating ferredoxin- and NAD-dependent [FeFe]-hydrogenase (HydABC) in *Moorella thermoacetica*. J Bacteriol 195:1267–1275. https://doi.org/10.1128/JB.02158-12
14. Wang S, Huang H, Moll J, Thauer RK. 2010. NADP+ reduction with reduced ferredoxin and NADP+ reduction with NADH are coupled via an electron-bifurcating enzyme complex in *Clostridium kluyveri*. J Bacteriol 192:5115–5123. https://doi.org/10.1128/JB.00612-10
15. Weghoff MC, Bertsch J, Müller V. 2015. A novel mode of lactate metabolism in strictly anaerobic bacteria. Environ Microbiol 17:670–677. https://doi.org/10.1111/1462-2920.12493
16. Duan HD, Lubner CE, Tokmina-Lukaszewska M, Gauss GH, Bothner B, King PW, Peters JW, Miller AF. 2018. Distinct properties underlie flavin-based electron bifurcation in a novel electron transfer flavoprotein FixAB from *Rhodopseudomonas palustris*. J Biol Chem 293:4688–4701. https://doi.org/10.1074/jbc.RA117.000707
17. Watanabe T, Pfeil-Gardiner O, Kahnt J, Koch J, Shima S, Murphy BJ. 2021. Three-megadalton complex of methanogenic electron-bifurcating and CO2-fixing enzymes. Science 373:1151–1156. https://doi.org/10.1126/science.abg5550
18. Kremp F, Roth J, Müller V. 2020. The Sporomusa type Nfn is a novel type of electron-bifurcating transhydrogenase that links the redox pools in acetogenic bacteria. Sci Rep 10:14872. https://doi.org/10.1038/s41598-020-71038-2
19. Tschech A, Pfennig N. 1984. Growth yield increase linked to caffeate reduction in *Acetobacterium woodii*. Arch Microbiol 137:163–167. https://doi.org/10.1007/BF00414460
20. Hansen B, Bokranz M, Schonheit P, Kroger A. 1988. ATP formation coupled to caffeate reduction by H2 in *Acetobacterium woodii* NZva16. Arch Microbiol 150:447–451. https://doi.org/10.1007/BF00422285

21. Imkamp F, Müller V. 2002. Chemiosmotic energy conservation with Na(+) as the coupling ion during hydrogen-dependent caffeate reduction by *Acetobacterium woodii*. J Bacteriol 184:1947–1951. https://doi.org/10.1128/JB.184.7.1947-1951.2002

22. Dilling S, Imkamp F, Schmidt S, Müller V. 2007. Regulation of caffeate respiration in the acetogenic bacterium *Acetobacterium woodii*. Appl Environ Microbiol 73:3630–3636. https://doi.org/10.1128/AEM.02060-06

23. Hess V, Vitt S, Müller V. 2011. A caffeyl-coenzyme a synthetase initiates caffeate activation prior to caffeate reduction in the acetogenic bacterium *Acetobacterium woodii*. J Bacteriol 193:971–978. https://doi.org/10.1128/JB.01126-10

24. Demmer JK, Bertsch J, Öppinger C, Wohlers H, Kayastha K, Demmer U, Ermler U, Müller V. 2018. Molecular basis of the flavin-based electron-bifurcating caffeyl-CoA reductase reaction. FEBS Lett 592:332–342. https://doi.org/10.1002/1873-3468.12971

25. Hess V, González JM, Parthasarathy A, Buckel W, Müller V. 2013. Caffeate respiration in the acetogenic bacterium *Acetobacterium woodii*: a coenzyme a loop saves energy for caffeate activation. Appl Environ Microbiol 79:1942–1947. https://doi.org/10.1128/AEM.03604-12

26. Bache R, Pfennig N. 1981. Selective isolation of *Acetobacterium woodii* on methoxylated aromatic acids and determination of growth yields. Arch Microbiol 130:255–261. https://doi.org/10.1007/BF00459530

27. Gulick AM. 2009. Conformational dynamics in the Acyl-CoA synthetases, adenylation domains of non-ribosomal peptide synthetases, and firefly luciferase. ACS Chem Biol 4:811–827. https://doi.org/10.1021/cb900156h

28. Robinson SL, Terlouw BR, Smith MD, Pidot SJ, Stinear TP, Medema MH, Wackett LP. 2020. Global analysis of adenylate-forming enzymes reveals β-lactone biosynthesis pathway in pathogenic *Nocardia*. J Biol Chem 295:14826–14839. https://doi.org/10.1074/jbc.RA120.013528

29. Arnold ME, Kaplieva-Dudek I, Heker I, Meckenstock RU. 2021. Aryl coenzyme a ligases, a subfamily of the adenylate-forming enzyme superfamily. Appl Environ Microbiol 87:e0069021. https://doi.org/10.1128/AEM.00690-21

30. Pande SV. 1973. Reversal by CoA of palmityl-CoA inhibition of long chain acyl-CoA synthetase activity. Biochim Biophys Acta 306:15–20. https://doi.org/10.1016/0005-2760(73)90202-6

31. Lin CY, Wang JP, Li Q, Chen HC, Liu J, Loziuk P, Song J, Williams C, Muddiman DC, Sederoff RR, Chiang VL. 2015. 4-Coumaroyl and caffeoyl shikimic acids inhibit 4-coumaric acid:coenzyme a ligases and modulate metabolic flux for 3-hydroxylation in monolignol biosynthesis of populus trichocarpa. Mol Plant 8:176–187. https://doi.org/10.1016/j.molp.2014.12.003

32. Lin C-Y, Sun Y, Song J, Chen H-C, Shi R, Yang C, Liu J, Tunlaya-Anukit S, Liu B, Loziuk PL, Williams CM, Muddiman DC, Lin Y-C, Sederoff RR, Wang JP, Chiang VL. 2021. Enzyme complexes of Ptr4CL and PtrHCT modulate co-enzyme a ligation of hydroxycinnamic acids for monolignol biosynthesis in *Populus trichocarpa*. Front Plant Sci 12:727932. https://doi.org/10.3389/fpls.2021.727932

33. Alberstein M, Eisenstein M, Abeliovich H. 2012. Removing allosteric feedback inhibition of tomato 4-coumarate:CoA ligase by directed evolution. Plant J 69:57–69. https://doi.org/10.1111/j.1365-313X.2011.04770.x

34. Leutwein C, Heider J. 2001. Succinyl-CoA:(R)-benzylsuccinate CoA-transferase: an enzyme of the anaerobic toluene catabolic pathway in denitrifying bacteria. J Bacteriol 183:4288–4295. https://doi.org/10.1128/JB.183.14.4288-4295.2001

35. Ricagno S, Jonsson S, Richards N, Lindqvist Y. 2003. Formyl-CoA transferase encloses the CoA binding site at the interface of an interlocked dimer. EMBO J 22:3210–3219. https://doi.org/10.1093/emboj/cdg333

36. Pandit SB, Bhadra R, Gowri VS, Balaji S, Anand B, Srinivasan N. 2004. SUPFAM: a database of sequence superfamilies of protein domains. BMC Bioinformatics 5:28. https://doi.org/10.1186/1471-2105-5-28

37. Atkinson HJ, Morris JH, Ferrin TE, Babbitt PC. 2009. Using sequence similarity networks for visualization of relationships across diverse protein superfamilies. PLoS ONE 4:e4345. https://doi.org/10.1371/journal.pone.0004345

38. Hackmann TJ, Firkins JL. 2015. Electron transport phosphorylation in rumen butyrivibrios: unprecedented ATP yield for glucose fermentation to butyrate. Front Microbiol 6:622. https://doi.org/10.3389/fmicb.2015.00622

39. Kaminsky RA, Reid PM, Altermann E, Kenters N, Kelly WJ, Noel SJ, Attwood GT, Janssen PH. 2023. Rumen *Lachnospiraceae* isolate NK3A20 exhibits metabolic flexibility in response to substrate and coculture with a methanogen. Appl Environ Microbiol 89:e0063423. https://doi.org/10.1128/aem.00634-23

40. Wu YT, Shen SJ, Liao KF, Huang CY. 2022. Dietary plant and animal protein sources oppositely modulate fecal *Bilophila* and *Lachnoclostridium* in vegetarians and omnivores. Microbiol Spectr 10:e0204721. https://doi.org/10.1128/spectrum.02047-21

41. Wiegel J, Tanner R, Rainey FA. 2006. An Introduction to the family clostridiaceae, p 654–678. In Dworkin M, Falkow S, Rosenberg E, Schleifer KH, Stackebrandt E (ed), The Prokaryotes: bacteria: firmicutes, cyanobacteria. Vol. 4. Springer, US New York, NY.

42. Haas KN, Blanchard JL. 2020. Reclassification of the *clostridium clostridioforme* and *clostridium sphenoides* clades as *Enterocloster gen*. nov. and *Lacrimispora gen*. nov., including reclassification of 15 taxa. Int J Syst Evol Microbiol 70:23–34. https://doi.org/10.1099/ijsem.0.003698

43. Lawson PA, Wawrik B, Allen TD, Johnson CN, Marks CR, Tanner RS, Harriman BH, Strąpoć D, Callaghan AV. 2014. *Youngiibacter fragilis* gen. nov., sp. nov., isolated from natural gas production-water and reclassification of acetivibrio multivorans as *Youngiibacter multivorans* comb. nov. Int J Syst Evol Microbiol 64:198–205. https://doi.org/10.1099/ijs.0.053728-0

44. Ivey KL, Chan AT, Izard J, Cassidy A, Rogers GB, Rimm EB. 2019. Role of dietary flavonoid compounds in driving patterns of microbial community assembly. MBio 10:e01205-19. https://doi.org/10.1128/mBio.01205-19

45. Kläring K, Just S, Lagkouvardos I, Hanske L, Haller D, Blaut M, Wenning M, Clavel T. 2015. *Murimonas intestini* gen. nov., sp. nov., an acetate-producing bacterium of the family *Lachnospiraceae* isolated from the mouse gut. Int J Syst Evol Microbiol 65:870–878. https://doi.org/10.1099/ijs.0.000030

46. Hu Y, Gai Y, Yin L, Wang X, Feng C, Feng L, Li D, Jiang XN, Wang DC. 2010. Crystal structures of a *Populus tomentosa* 4-coumarate:CoA ligase shed light on its enzymatic mechanisms. Pl Cell 22:3093–3104. https://doi.org/10.1105/tpc.109.072652

47. Obel N, Scheller HV. 2000. Enzymatic synthesis and purification of caffeoyl-CoA, p-coumaroyl-CoA, and feruloyl-CoA. Anal Biochem 286:38–44. https://doi.org/10.1006/abio.2000.4760

48. Altschul SF, Madden TL, Schäffer AA, Zhang J, Zhang Z, Miller W, Lipman DJ. 1997. Gapped BLAST and PSI-BLAST: a new generation of protein database search programs. Nucleic Acids Res 25:3389–3402. https://doi.org/10.1093/nar/25.17.3389

49. Tietz JI, Schwalen CJ, Patel PS, Maxson T, Blair PM, Tai HC, Zakai UI, Mitchell DA. 2017. A new genome-mining tool redefines the lasso peptide biosynthetic landscape. Nat Chem Biol 13:470–478. https://doi.org/10.1038/nchembio.2319

50. Guy L, Kultima JR, Andersson SGE. 2010. genoPlotR: comparative gene and genome visualization in R. Bioinformatics 26:2334–2335. https://doi.org/10.1093/bioinformatics/btq413